Draft version November 1, 2022
Typeset using LaTeX **twocolumn** style in AASTeX62

The Density Profiles of Collapsed Rotating Massive Stars Favor Long Gamma-Ray Bursts

Goni Halevi,[1,2] Belinda Wu,[1] Alexander Tchekhovskoy,[3] David R. Aguilera-Dena,[4] Philipp Mösta,[5] and Ore Gottlieb[6]

[1] *Department of Astrophysical Sciences, Princeton University, 4 Ivy Lane, Princeton, NJ 08544, USA*
[2] *Institute For Advanced Study, 1 Einstein Drive, Princeton, NJ 08540, USA*
[3] *Center for Interdisciplinary Exploration & Research in Astrophysics (CIERA), Physics & Astronomy, Northwestern University, Evanston, IL 60201, USA*
[4] *Institute of Astrophysics, FORTH, Dept. of Physics, University of Crete, Voutes, University Campus, GR-71003 Heraklion, Greece*
[5] *GRAPPA, Anton Pannekoek Institute for Astronomy and Institute of High-Energy Physics, University of Amsterdam, Science Park 904, 1098 XH Amsterdam, The Netherlands*
[6] *Center for Interdisciplinary Exploration Research in Astrophysics (CIERA), Physics Astronomy, Northwestern University, Evanston, IL 60201, USA*

(Received XX; Revised XX; Accepted XX)

Submitted to ApJL

ABSTRACT

Long-duration gamma-ray bursts (lGRBs) originate in relativistic collimated outflows – jets – that drill their way out of collapsing massive stars. Accurately modeling this process requires realistic post-collapse stellar profiles for the jets to propagate through and break out of. Most previous studies have used simple power laws in place of well-motivated stellar progenitor models. To develop such models, we use the one-dimensional open-source code GR1D to simulate the core-collapse process for a suite of low-metallicity, rotating, massive stellar progenitors that have undergone chemically homogeneous evolution. The models we evolve span a range of zero-age-main-sequence (ZAMS) masses: $M_{\rm ZAMS}$ = 13, 18, 21, 25, 35, 40, and 45 $M_\odot$. We follow four out of our seven models until they collapse to form black holes (BHs), while the other three form proto-neutron stars (PNSs). We robustly find, across all models, that the final density profile outside of the newly formed BH or PNS is well-represented by a power law with an index of $\alpha \approx 1.2-1.5$. Our fiducial $M_{\rm ZAMS} = 18M_\odot$ model has a late-time power law index of $\alpha \approx 1.45$. These profiles are consistent with stellar progenitors conducive to successful formation, propagation, and breakout of BH-powered jets and the resulting lGRBs.

Keywords: magnetohydrodynamics — stellar mass black holes — gamma-ray bursts — core-collapse supernovae

1. INTRODUCTION

2. METHODS

2.1. *Pre-collapse stellar models*

For our initial conditions, we begin with the pre-collapse stellar models described in Aguilera-Dena et al. (2020) (hereafter AD20). We now summarize the basic physics of the AD20 suite of models.

AD20 presents the evolved states of stellar progenitors across the initial mass range for massive, low-metallicity stars, spanning zero-age-main-sequence (ZAMS) masses of $M_{\rm ZAMS} = 4-45M_\odot$. The models are computed using the open-source one-dimensional stellar evolution Modules for Experiments in Stellar Astrophysics in version 10398 (MESA; Paxton et al. 2011, 2013, 2015, 2018). Each star is initialized with (1) a rapid equatorial rotational velocity of 600 km s^{-1} and (2) a low metallicity of $(1/50)Z_\odot$, where $Z_\odot$ represents solar metallicity and abundances are scaled from Grevesse et al. (1996). The fast initial rotation guarantees effective mixing leading to quasi-chemically homogenous evolution. Such models are motivated by suggestions that, if they collapse to form BHs, they would produce lGRBs and associated energetic stripped-envelope supernovae (SNe) known as

Corresponding author: Goni Halevi
ghalevi@princeton.edu

Type Ic-BLs under the collapsar model of MacFadyen & Woosley (1999). On the other hand, models that fail to form BHs could instead leave behind millisecond magnetars that may continuously deposit energy into the ejecta during spin-down, powering superluminous supernovae (SLSNe; Kasen & Bildsten 2010; Woosley 2010; Metzger et al. 2015; Nicholl et al. 2017).

We evolve seven different models from the set of 42 included in AD20, spanning a range of initial masses and expected explosion properties. We choose the $M_{\rm ZAMS} = 18M_\odot$ model as our fiducial model because it is most similar, at the onset of core-collapse, to the well-studied lGRB progenitor model 16Ti of Woosley & Heger (2006). It has a similar mass of $14.15M_\odot$ (compared to $13.95M_\odot$ for 16Ti) at the onset of core collapse due to mass loss dominated by rotation, which is enhanced by neutrino-driven contraction. The $M_{\rm ZAMS} = 18M_\odot$ stellar model is classified by AD20 as a likely failed supernova and potential lGRB progenitor based on its distance from various explosion criteria. The simplest of these is the compactness parameter, which is motivated by hydrodynamic simulations of neutrino-driven SNe and defined as

$$\xi_M = \frac{M/M_\odot}{R(M_{\rm bary} = M)/1000\ {\rm km}}, \quad (1)$$

where $M_{\rm bary}$ is the enclosed baryonic mass. This single-parameter estimate is commonly used as an indicator of 'explodability'– whether or not a non-rotating stellar core will lead to a successful neutrino-driven explosion. It is often measured at a mass coordinate of 2.5 $M_\odot$, which corresponds to a typical infall velocity of 1000 km s^{-1}. Non-rotating cores with $\xi_{2.5} \gtrsim 0.45$ are predicted to be difficult to successfully explode, as calibrated by core-collapse simulations (Sukhbold & Woosley 2014). Our fiducial model has $\xi_{2.5} = 0.62$. All of the models we present here, except for the lowest mass ($M_{\rm ZAMS} = 13M_\odot$) one, have compactness parameters above 0.45 and are therefore expected by this simple explodability predictor to fail to explode and to instead collapse to form BHs.

Figure 1 shows radial profiles of density, temperature, radial velocity, and angular velocity at this time for the fiducial $M_{\rm ZAMS} = 18M_\odot$ model along with the other six models. We include the initial parameters for each of these models, as taken from AD20, in the first few columns of Table 1. In particular, we list the stellar mass at the onset of core-collapse (defined as the time when the core infall velocities first exceed 1000 km s^{-1}) $M_{\rm pre-cc}$ and the compactness parameter $\xi_{2.5}$. We note that while there are many similarities between the different models, there are also non-linear differences between them, for example in the rotational velocities of their core regions (see Figure 1d). This is also reflected in the non-monotonic (as a function of stellar mass) behavior of $\xi_{2.5}$.

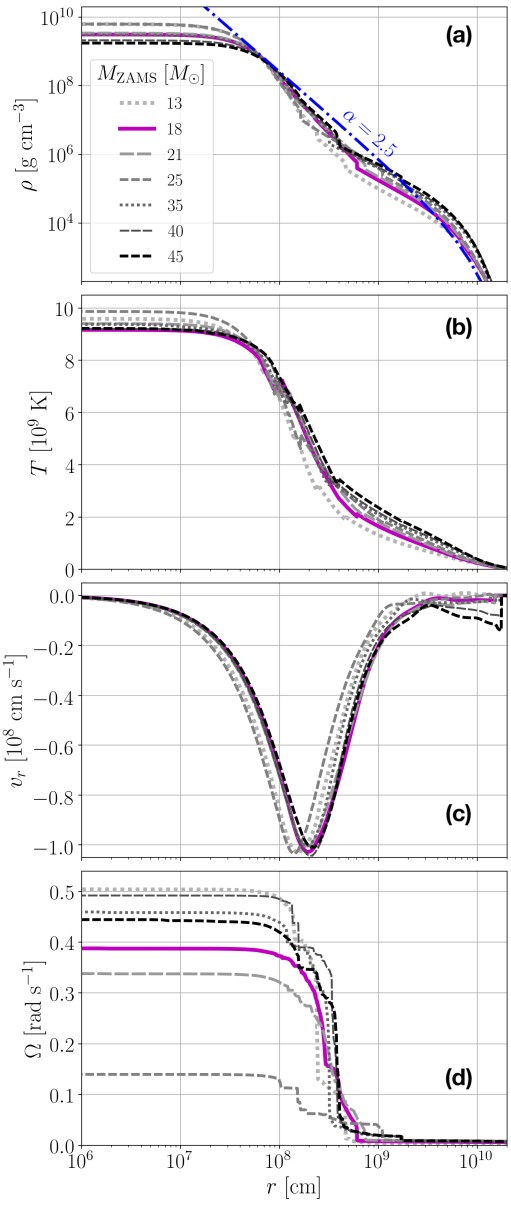

Figure 1. Stellar properties as a function of radius for the one-dimensional MESA models of Aguilera-Dena et al. (2020). In the four panels, we show (a) mass density, (b) temperature, (c) radial velocity, and (d) angular velocity. The different mass models are represented by different color and style lines as labeled, with the fiducial $M_{\rm ZAMS} = 18M_\odot$ model in solid magneta. We also include, in blue, a fit to Equation 2 with $\alpha = 2.5$. All models share similar density, temperature, and radial velocity profiles. Their core rotational velocities differ by a up to about 40% and vary non-monotonically with ZAMS mass.

Besides the $13M_\odot$ one, all of the models we adopt fail to meet the explosion criterion of Müller et al. (2016), which predicts properties of neutrino-driven explosions

$M_{\rm ZAMS}$ ($M_\odot$)	$M_{\rm pre-cc}$ ($M_\odot$)	$\xi_{2.5}$	$t_{\rm bounce}$ (ms)	t_f (s)	$M_{\rm core}$ ($M_\odot$)	α
13	10.37	0.21	152	0.83	2.03	1.42
18	14.15	0.62	234	0.74	2.45	1.45
21	16.39	0.66	216	0.72	2.44	1.40
25	19.33	0.47	152	0.77	2.08	1.28
35	26.53	0.57	247	0.83	2.40	1.24
40	30.08	0.78	258	0.74	2.68	1.41
45	33.59	0.85	285	0.61	2.63	1.50

Table 1. Parameters of the stellar models. We take the following pre-collapse quantities directly from AD20: ZAMS mass $M_{\rm ZAMS}$, mass at the time of re-mapping to GR1D $M_{\rm pre-cc}$, and compactness parameter at this time $\xi_{2.5}$ as defined in Equation 1. We add to these the time of core-bounce in our GR1D simulations $t_{\rm bounce}$ and final quantities at the end of the simulation, which occurs at t_f: the mass of the inner core $M_{\rm core}$ and best-fit power-law index for the density profile α.

based on a semi-analytic model for stellar structure. Both the least ($13M_\odot$) and most massive ($45M_\odot$) models are predicted to explode based on the Ertl et al. (2016) test, which employs a two-parameter representation of stellar structure, while the rest fail to meet this criterion as well. These predictions are also not monotonic with initial or pre-collapse mass due to the complexities of stellar evolution. We include the $M_{\rm ZAMS} = 13M_\odot$ model as a comparison point to the failed supernovae, but from the perspective of likely lGRB progenitors, we focus on the more massive models.

2.2. *Core-collapse simulations*

We map each model onto GR1D (GR1D; O'Connor & Ott 2010), another spherically-symmetric code, in order to evolve through the final stage of stellar evolution. GR1D is an open-source tool[1] for simulating core-collapse and black hole formation. It uses a finite-volume scheme with piecewise-parabolic reconstruction and a Riemann solver to solve the discretized equations of general-relativistic hydrodynamics (GRHD). It couples with microphysical, tabulated equations of state and includes an approximate treatment of rotation. It too is a modular code and, crucially, implements neutrino transport in the M1 formulation (O'Connor 2015) with tabulated multi-group neutrino opacities. Although spherically symmetric models can never fully capture the three-dimensional complexity of stellar evolution (e.g. critically-rotating stars are expected to be significantly oblate), for the purpose of determining the ultimate fate of this star, its remnant mass, and its average thermodynamic radial profiles, GR1D is a useful and sufficient tool. It allows us to simulate the entire star rather than collapsing only the inner-region. This is critical for understanding the environment that a collimated outflow from the accreting newborn compact object must drill through and break out of in order to power a lGRB.

The initial conditions for our GR1D simulations are the pre-collapse models of AD20. In particular, we map the following parameters (as a function of radial coordinate) onto a new grid: enclosed mass, temperature, density, radial velocity, electron fraction, and angular velocity. We choose a grid for our models that is uniform ($\Delta r = 100$ m) in the inner region (up to 2 km) and logarithmically spaced outside of it, with a total of 1200 radial zones (in addition to ghost zones). The grid extends out to where the density has dropped below 2000 g cm^{-3}. The remapping for each model is done at the time when it has reached a maximum core infall velocity of $v_r > 1000$ km s^{-1}, representing the onset of core-collapse. The masses of the stars at this time, $M_{\rm pre-cc}$ are included in the third column of Table 1.

We choose a commonly-used tabulated equation of state appropriate for hot nuclear matter from Lattimer & Swesty (1991) with an incompressibility of $K_{\rm sat} = 220$ MeV (known as LS220). We include 3 species of neutrinos and evolve them out to 600 km. Their opacities are tabulated and include 18 energy groups and a large parameter space of thermodynamic quantities.

3. RESULTS

3.1. *Core-collapse evolution*

All models evolve qualitatively similarly for the first few hundred milliseconds of their evolution. The fiducial $M_{\rm ZAMS} = 18M_\odot$ model along with the $M_{\rm ZAMS} = 21$, 40, and 45 $M_\odot$ ones all collapse to form black holes. Every model in this set follows similar evolution. On the other hand, the $M_{\rm ZAMS} = 13$, 25, and 35 $M_\odot$ models all fail to form black holes and may be representative of successful neutrino-driven supernova explosions. To represent these two different outcomes, we show the density and radial velocity profiles for the $M_{\rm ZAMS} = 18$ and 13 $M_\odot$ models at multiple stages of their evolution in Figure 2.

During collapse, the outer envelope of the star ($r \gtrsim 4\times10^{10}$ cm) is largely unaffected due to causality, while the inner region falls inward, making the core increasingly compact. Nuclear and residual strong forces in the dense core lead to the production of a proto-neutron star (PNS) and drive a shock outward at at time $t_{\rm bounce}$ (known as core-bounce). We include snapshots from just before and just after this time in Figure 2.

[1] https://github.com/evanoconnor/GR1D

At $t < t_{\rm bounce}$, infalling material steepens into a shock and there is a sharp drop in density outside the core and a correspondingly sharp negative velocity at the same radius ($r \approx 10$ km). At $t > t_{\rm bounce}$, the shock moves outward as neutrinos are released in the core and heat the region behind it. This is reflected in the positive velocities at the boundary of the newly formed PNS and then outward movement of the shock.

Eventually, however, the shock stalls and falls back, leading to the infall of the shock as seen in Figure 2 for the $M_{\rm ZAMS} = 18$ and 13 $M_\odot$ models. For the former, our fiducial model, core-bounce occurs at $t_{\rm bounce} = 234$ ms. Approximately half of a second later, the PNS itself begins to collapse to form a BH, marking the end of the simulation. This is reflected in a rapid increase of the density in the inner regions and negative radial velocities appearing within the PNS boundary. We end our simulations at this time because GR1D can no longer evolve the metric once the central density exceeds a certain level (dependent on the choice of metric). We list the times of core bounce $t_{\rm bounce}$ and the final simulation time t_f for all models in Table 1.

3.2. *Remnants*

The central density as a function of time after core-bounce is shown for each simulation in the top panel of Figure 3. For all models, the core density grows steadily after bounce as the core continues to accrete mass. The $M_{\rm ZAMS} = 18M_\odot$, $21M_\odot$, $40M_\odot$, and $45M_\odot$ models all accrete enough matter to experience runaway gravitational collapse. At this point, the central density rises exponentially, indicating the onset of black hole formation. The maximum neutron star mass is a function of both the equation of state and the angular momentum of the core.

In each of our seven models, a shock wave is driven outward from the core at the time of core-bounce. However, it stalls and turns back within 100 ms for all models as fallback accretion occurs. The $M_{\rm ZAMS} = 13$ and 25 $M_\odot$ models both experience a brief shock revival from neutrino heating but still eventually undergo a reversal and fallback accretion, as seen in the middle panel of Figure 3. These two models also have the smallest enclosed mass within the shock radius and are thus least likely to collapse to form BHs. The $M_{\rm ZAMS} = 35M_\odot$ model also fails to collapse to a BH by the end of our simulations. It is possible that in longer simulations, these PNSs would collapse, especially for the $M_{\rm ZAMS} = 35M_\odot$ model which has the most massive core of the three.

The rate at which the inner core mass increases slows with time for each of the seven simulations as the accretion rates fall. Each model forms a core of mass $2M_\odot < M_{\rm core} < 2.7M_\odot$ by the end of the simulation, as shown in both Table 1 and the bottom panel of Figure 3. The core mass is defined as the mass within the radius at which the radial velocity first exceeds the sound speed, $r_{\rm shock}$. In all cases, $M_{\rm core}$ represents the minimum mass for the final remnants, as the cores are expected to continue accreting matter after the end of our simulations.

3.3. *Density profiles*

For each of the seven simulations, we find that the density profile after core-collapse is well-fit by a distribution of the form:

$$\rho(r) = \rho_0 \left(\frac{r}{r_g}\right)^{-\alpha} \left(1 - \frac{r}{R_\star}\right)^3 \qquad (2)$$

where ρ_0 is the normalization factor satisfying $M_\star = \int_0^{R_\star} \rho(r) dV$, r_g is the gravitational radius of the remnant, and $R_\star$ is the stellar radius.

The initial density profiles are similar across stellar masses with best-fit power-law indices of $\alpha \approx 2.5$. In all cases, the density profile becomes shallower during core-collapse, and especially in the time after the shock stalls and turns around. The final density and pressure profiles are very smooth in the region 20 km $\lesssim r \lesssim$ 2000 km. For our fiducial collapsed stellar model at the end of the GR1D simulation, we find a best-fit value of $\alpha = 1.45$ for the density outside of the black hole event horizon. We include the best-fit value of α for all models in the final column of Table 1. They vary non-monotonically with mass and range from 1.24 for the $M_{\rm ZAMS} = 35M_\odot$ model to 1.50 for the $M_{\rm ZAMS} = 45M_\odot$ model. We compare the density profiles for all seven models at the beginning and end of their GR1D simulations in Figure 4.

4. DISCUSSION AND CONCLUSION

Power-law density profiles with indices of $\alpha \approx 1.5$ are consistent with the simple case of free-fall acceleration outside the core. The pressure distributions are well-fit with slightly steeper power-laws across all models, reflecting the steeper initial distributions in pressure. They are also consistent with free-fall. This makes it all the more meaningful that our GR1D simulations yield this robust result for the final state of all models. The initial models have non-linear differences in their stellar structure, so there are complicated variations in the inputs to GR1D. These differences are mainly related to whether core carbon burning proceeds radiatively or convectively. Meanwhile, the physics that enters these one-dimensional simulations is complex in that we simulate collapse in full general-relativity, with multi-group neutrino transport and realistic tabulated equations of

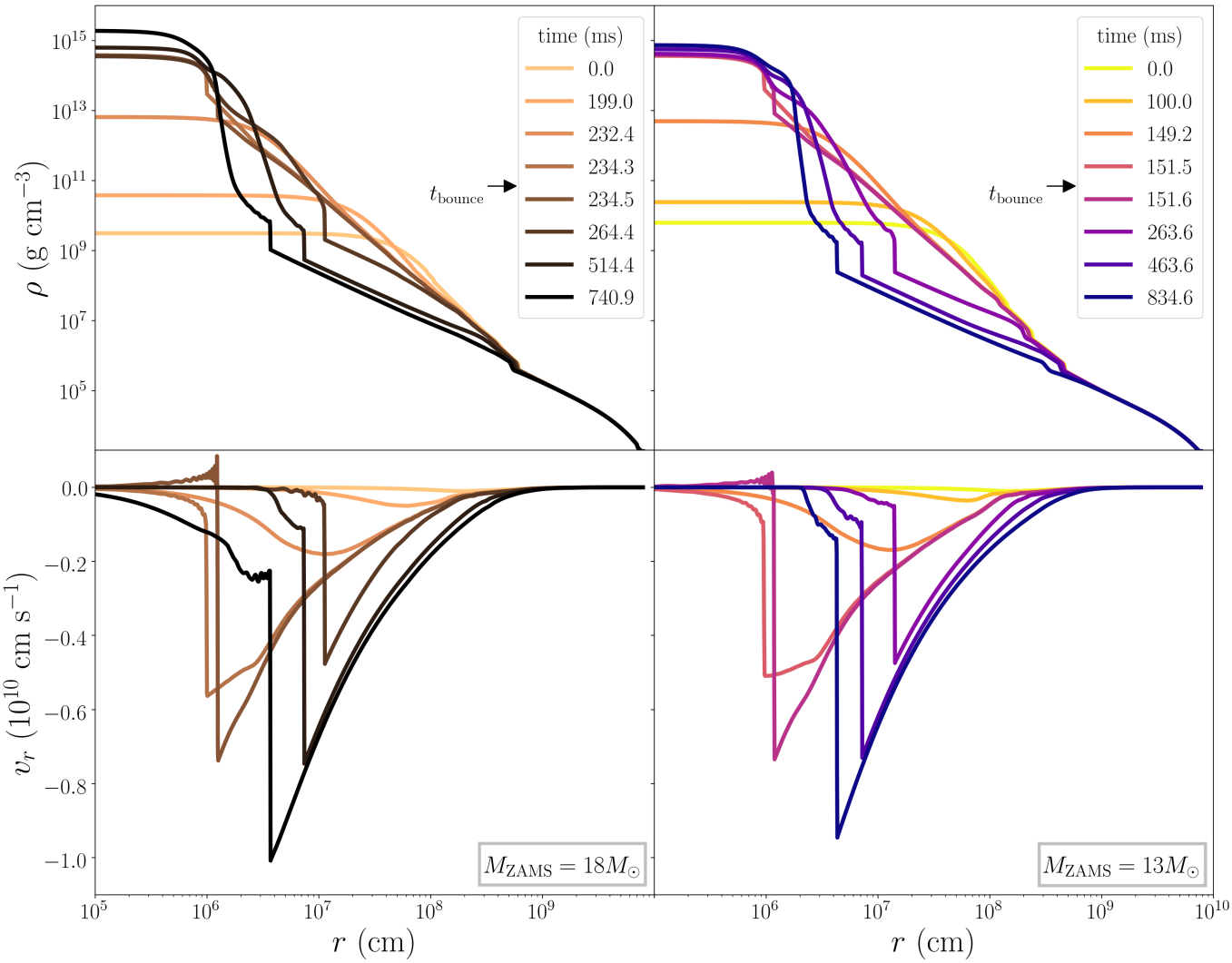

Figure 2. Evolution of the density and velocity profiles (in top and bottom panels, respectively) of the $M_{\rm ZAMS} = 18M_\odot$ and $13M_\odot$ models (left and right, respectively) during GR1D evolution through core collapse. The $18M_\odot$ model forms a black hole at the end of its evolution, as evidenced by the infall seen within the core in the final snapshot, whereas the $13M_\odot$ model does not.

state suitable for dense matter. These ingredients are necessary to drive the evolution that leads to this superficially simple outcome.

4.1. *Applications for long GRBs*

The consequences of the precise density profiles we find in our one-dimensional core-collapse simulations of real stellar progenitor models are favorable for producing long GRBs. Three-dimensional GRMHD simulations of collapsars have followed the formation and break-out of jets (Gottlieb et al. 2022a,b). These simulations begin with idealized initial conditions of a central black hole surrounded by an effectively zero-temperature star represented by an analytic power-law density profile as in Equation 2. Dipolar magnetic fields and fast rotational velocities are then added to the idealized stellar profile, leading to accretion, a build-up of magnetic flux at the horizon, and the launching of a jet that propagates through the stellar envelope. Gottlieb et al. (2022a) varied the initial power-law index α and compared the physical quantities inferred from the resulting jets to observational constraints. They conclude that inner stellar density profiles with indices of $0.5 \lesssim \alpha \lesssim 1.5$ may be responsible for producing the full range of long GRB observables. In particular, such profiles are found to be necessary to produce jets with the proper luminosities, engine durations, and (flat) evolution in jet power with time. On the other hand, density profiles like those of pre-collapse models 16Ti (Woosley & Heger 2006) or the models presented in this work have steeper profiles of $\alpha \approx 2.5$. Such profiles would require too luminous of jets to overcome accretion and break out ($L \gtrsim 10^{52}$ erg s^{-1})

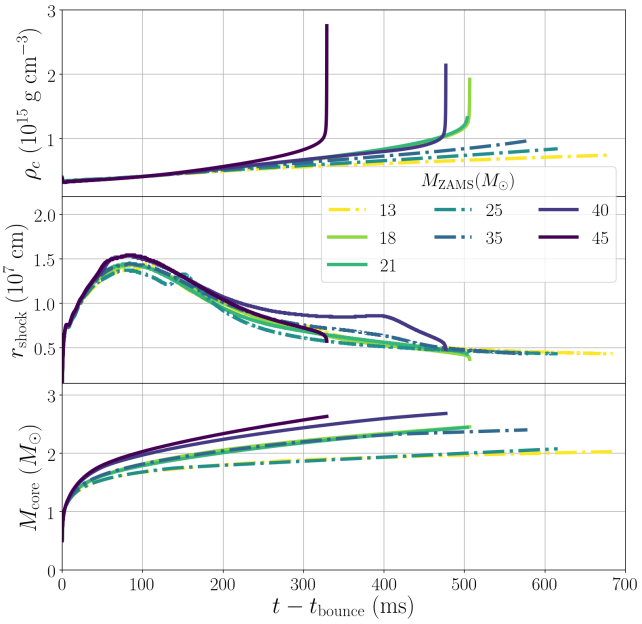

Figure 3. Evolution of several key quantities (from top to bottom: central density, shock radius, and mass of the inner core) with time after core bounce for all seven models. The shock radius $r_{\rm shock}$ is defined as the place where the radial velocity exceeds the sound speed and the inner core is the region within this radius, so $M_{\rm core} \equiv M(r < r_{\rm shock})$. Models that form BHs in our simulations are represented by solid lines while models that do not are shown as dash-dotted lines.

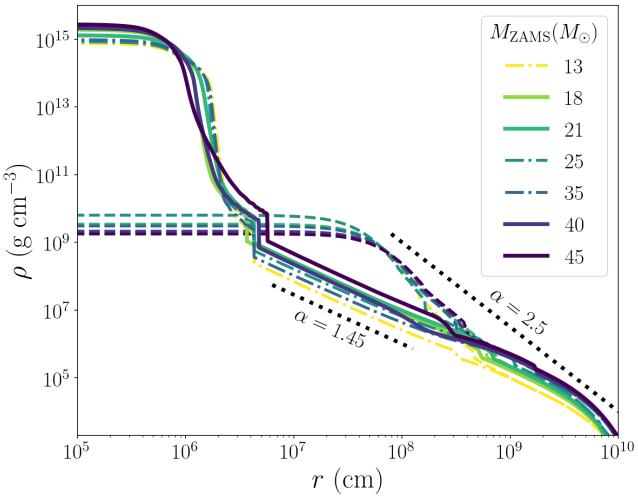

Figure 4. Initial (pre-core-collapse) and final density profiles for all seven stellar models. Initial profiles are shown as dashed lines. For the final profiles, we use solid lines for models that collapse to form BHs in our simulations and dash-dotted lines for those that do not. Representative power-law scalings with indices of 2.5 and 1.45 are shown in dotted black lines for comparison to initial and final profiles, respectively.

and rising light curves. This conclusion is consistent with the stellar models presented here, which were chosen as long GRB progenitor candidates.

With these post-black hole formation stellar models from the end of our GR1D simulations, we can initialize three-dimensional GRMHD simulation self-consistently. This will allow us to confirm that specific stellar progenitors as modeled in MESA through their entire stellar evolution processes and collapsed in GR1D can indeed go on to successfully launch jets that are consistent with long GRB observables.

We thank Evan O'Connor for his generosity and guidance in using GR1D. G.H. is supported in part by a National Science Foundation Graduate Research Fellowship.

REFERENCES

Aguilera-Dena, D. R., Langer, N., Antoniadis, J., & Müller, B. 2020, ApJ, 901, 114

Ertl, T., Janka, H. T., Woosley, S. E., Sukhbold, T., & Ugliano, M. 2016, ApJ, 818, 124

Gottlieb, O., Lalakos, A., Bromberg, O., Liska, M., & Tchekhovskoy, A. 2022a, MNRAS, 510, 4962

Gottlieb, O., Liska, M., Tchekhovskoy, A., et al. 2022b, ApJL, 933, L9

Grevesse, N., Noels, A., & Sauval, A. J. 1996, in Astronomical Society of the Pacific Conference Series, Vol. 99, Cosmic Abundances, ed. S. S. Holt & G. Sonneborn, 117

Kasen, D., & Bildsten, L. 2010, ApJ, 717, 245

Lattimer, J. M., & Swesty, D. F. 1991, NuPhA, 535, 331

MacFadyen, A. I., & Woosley, S. E. 1999, ApJ, 524, 262

Metzger, B. D., Margalit, B., Kasen, D., & Quataert, E. 2015, MNRAS, 454, 3311

Müller, B., Heger, A., Liptai, D., & Cameron, J. B. 2016, MNRAS, 460, 742

Nicholl, M., Guillochon, J., & Berger, E. 2017, ApJ, 850, 55

O'Connor, E. 2015, ApJS, 219, 24

O'Connor, E., & Ott, C. D. 2010, Classical and Quantum Gravity, 27, 114103

Paxton, B., Bildsten, L., Dotter, A., et al. 2011, ApJS, 192, 3

Paxton, B., Cantiello, M., Arras, P., et al. 2013, ApJS, 208, 4

Paxton, B., Marchant, P., Schwab, J., et al. 2015, ApJS, 220, 15

Paxton, B., Schwab, J., Bauer, E. B., et al. 2018, ApJS, 234, 34

Sukhbold, T., & Woosley, S. E. 2014, ApJ, 783, 10

Woosley, S. E. 2010, ApJL, 719, L204

Woosley, S. E., & Heger, A. 2006, ApJ, 637, 914